Generation of Bessel beams using a magnetic liquid deformable mirror

Denis Brousseau,* Julie Drapeau, Michel Piché, and Ermanno F. Borra

Center for Optics, Photonics and Lasers (COPL), Laval University, Quebec, Canada, G1V 0A6

*Corresponding author: denis.brousseau@copl.ulaval.ca

Received 12 May 2011; revised 10 June 2011; accepted 15 June 2011;
posted 16 June 2011 (Doc. ID 147309); published 14 July 2011

A deformable mirror made of a magnetic liquid has been used to produce conical surfaces with subwavelength ($\lambda/4$) accuracy. The surface profile of the liquid mirror is controlled by 91 small magnetic coils. The mirror exhibits a linear response with respect to the currents driving the coils, and it allows for real-time changes of its surface profile. The magnetic liquid deformable mirror has been used to produce reflected beams having a conical wavefront; the propagation of the reflected beams was verified to be consistent with that of Bessel beams in the near and far field. The large dynamic range of such a deformable mirror has made it possible to generate Bessel beams with a broad range of beam parameters. © 2011 Optical Society of America

OCIS codes: 230.4040, 110.1080.

1. Introduction

Bessel beams have a long history that can be traced back to the early works on super-resolution. It was then known that an annular beam would produce a focused field described by a Bessel function that could exhibit enhanced spatial resolution [1]. Bessel beams were later introduced by Durnin *et al.* [2] in order to take advantage of their apparent "diffraction-free" character. This latter contribution triggered an immense interest for the generation and characterization of Bessel beams as well as for their application in various areas. The so-called "diffraction-free" property of Bessel beams stems from the fact that they exhibit a narrow central spot that extends over a collimation length L_c much longer than the Rayleigh range that could be associated with that spot. A most interesting feature of Bessel beams is their property of self-reconstruction beyond an obstacle [3]. That property has recently been exploited to reduce scattering artifacts and enhance image quality and penetration depth in dense media [4]. Bessel beams have also been used in the manipulation of atoms and microparticles [5,6], in optical testing of surfaces and wavefront sensing [7,8], to enhance the depth of field of one- and two-photon microscopy [9,10], and in the fabrication of optical waveguides [11], among others. The concept of diffraction-free beams has been extended to the temporal domain where dispersion plays a role similar to diffraction in the spatial domain; this has led to the investigation of wave packets such as X- and O-waves [12] and spatiotemporal Bessel beams [13] that exhibit interesting space–time coupling phenomena. Recent developments include Airy beams that provide focal lines with a curved trajectory [14].

The original scheme introduced by Durnin *et al.* [2] to produce Bessel beams consisted of using an annular mask and a Fourier transform lens; however, this approach is inefficient due to the low transmission of the mask. Other methods can produce Bessel beams with an excellent efficiency. The most common method is based on refractive axicons that take the shape of conical surfaces built from dielectrics [15]. Beam-shaping elements based on diffractive optics or holography have also been developed [16,17]. Refractive axicons allow generating Bessel beams of excellent quality with beam parameters selected by the cone angle and incident beam size. However, an axicon can only produce Bessel beams with a specific spatial

0003-6935/11/214005-06$15.00/0

frequency, hence, with a predetermined central spot. This is due to the fact that a Bessel beam is built through the interference of plane waves that are all refracted by the same deflection angle β; in turn, this angle fixes the value of the collimation length $L_c = \rho_{in}/\beta$, where ρ_{in} is the radius of the beam incident on the axicon. To circumvent the problem of a fixed deflection angle, spatial light modulators and acousto-optic elements have been used to generate Bessel beams [18–21]; however, these methods are often subject to pixelation and chromatic aberrations. Bessel beams can also be produced by reflective elements as demonstrated in [22], where a metallic axicon mirror is described. An adjustable conical surface made through the application of a pressure at the center of a membrane has also been reported in [23]. In the following paper, we present a different approach and take advantage of the flexibility and excellent performance offered by magnetic liquid deformable mirrors (MLDMs) to generate Bessel beams.

2. Magnetic Liquid Deformable Mirrors and Experimental Setup

MLDMs are deformable mirrors based on the magnetic actuation of the surface of a magnetic liquid (ferrofluid). The magnetic field that shapes the surface of the liquid is produced by small current-carrying coils. MLDMs have been introduced by our group in 2004 [24] and several progresses have been made since then. In early prototypes, the necessity to sum each magnetic field vector component independently prohibited linear addition of the influence functions of the mirror to predict and control the surfaces produced by MLDMs. A major advancement that was recently achieved is that we successfully countered this problem. The nonvectorial behavior is obtained using a new technique that superimposes a large and uniform magnetic field to the magnetic field produced by the array of small coils. A thorough description of this technique and experimental results can be found in [25] and [26]. In the following paragraphs, we briefly describe the characteristics of the MLDM and the method that were used in this paper.

A. Experimental Setup

The MLDM used to produce conical surfaces consists of 91 2.8 mm diameter custom coils disposed into a 33 mm diameter hexagonal array. Each resin-coated coil consists of roughly 300 turns of 0.13 mm diameter magnet wire wound on a 1 mm diameter brass core. The coils are supplied in current by a custom amplifying stage that converts the −10 to +10 V of a 96 channel PCI card to a current ranging from −200 to +200 mA. The external magnetic field that linearizes the response of the actuators is produced by a Maxwell bobbin [27]. The coil array is placed within the Maxwell bobbin with the top portion of the coils lying near the middle of the Maxwell bobbin form, a position where the magnetic field produced by the bobbin is uniform. A container filled with a 1 mm deep layer of commercial EFH1 ferrofluid from Ferrotec Corp. sits on top of the coils. A circular antireflective-coated 50 mm diameter optical-quality BK7 window is used to protect the liquid surface from dust particles and air currents from the room air exchange system. During normal operation, the Maxwell bobbin is driven with a constant current of 0.8 A.

Figure 1 shows a schematic representation of the experimental setup. Light from a laser diode (LD) at 659.5 nm is filtered by a spatial filter (SF) composed of a 10× microscope objective and a 25 μm pinhole. The single lobe beam pattern is collimated to a 25 mm diameter beam by lens L1 ($f = 250$ mm) that illuminates the surface of the MLDM using a beam splitter (BS) and a folding mirror (not shown). The light reflected back from the MLDM then goes through a $1/5\times$ telescope formed by the L2/L3 lens combination where it can then be recorded using two different instruments by means of a removable folding mirror (M). An 8 bit Lumenera Lu175 complementary metal–oxide–semiconductor (CMOS) camera having 1280 5.2μm pixels × 1024 5.2 μm pixels is used to record the Bessel beams and far-field images. The surface profile of the mirror can be analyzed using a Shack–Hartmann wavefront sensor (WFS) from Imagine Optic having 44 microlenses × 44 microlenses with a pitch of 114 μm. The WFS microlens array is positioned at the conjugate image plane of the MLDM. Lens L4 is used to record the far-field image and is removed to record the Bessel beam profiles.

B. Method

The coil currents required to produce an axicon are computed using the following standard method. A surface **w** produced by the MLDM can be represented as a linear combination of the individual response functions of the coils in the matrix form

$$\mathbf{w} = \mathbf{Ha}, \tag{1}$$

where **H** is called the influence matrix and **a** is a vector of the coil currents. Each column of the control matrix **H** represents the response function (influence

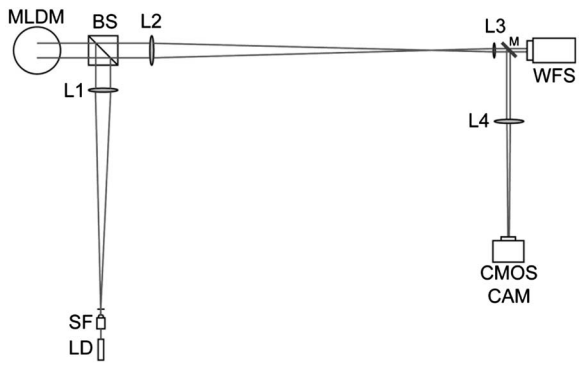

Fig. 1. Layout of the experimental setup.

function) of a single coil shifted to its corresponding location on the hexagonal grid, while each row of **H** corresponds to a single surface data sample. The matrix **H** needs to have more rows (data samples) than columns (coils). The solution for minimum variance of Eq. (1) gives the following current vector to be supplied to the coil array of the MLDM:

$$\mathbf{a} = (\mathbf{H}^t\mathbf{H})^{-1}\mathbf{H}^t\mathbf{w}, \tag{2}$$

where the superscript t denotes the transpose matrix operation. The influence function of each coil is recorded using the WFS. The 91 recorded influence functions are used to construct an experimental matrix **H** and the currents to produce an axicon can then be computed using Eq. (2) and singular value decomposition. The currents are supplied to the coils and the surface produced by the axicon is recorded using the WFS. A current adjustment is then computed from the difference between the targeted and the measured surfaces. This current adjustment is then added to the original currents and the new current vector is supplied again to the coils. Iterations on the currents are made until the residual ceases to decrease, which usually occurs after two to six iterations. A major advantage resulting from having a linear response (the surface amplitude produced by a single coil is directly proportional to its driving current) is that when a set of currents has been optimized for a specific cone angle value, other cone angles can easily be produced by a simple scaling of the currents as shown in [25] for a common defocus optical aberration. This property has been used here to produce axicons having different cone angles.

3. Results

The setup has been used to generate axicons with a wide range of values of the cone angle α. With a reflective axicon, the angle β of the conical beam reflected by the axicon is $\beta = 2\alpha$. At the output of the telescope, the beam is still a Bessel beam but the angles are scaled according to $f_3 \tan(\beta') = f_2 \tan(\beta)$, where f_3 and f_2 are the focal length of lenses L3 and L2. As the angles are small, the above relation becomes $\beta \simeq \beta'(f_3/f_2) = \beta'/5$. The spatial profile of a Bessel beam produced by an axicon with $\alpha = 0.5$ mrad and imaged by the CMOS camera is shown in Fig. 2 at various positions along the propagation (z) axis after it has passed through the L2/L3 telescope. One clearly observes a pattern made of concentric annular rings with an intense central spot. The structure of the pattern is invariant along the z-axis, illustrating the "diffraction-free" character of the produced Bessel beams as seen in Fig. 3, which displays three experimental patterns fitted using a Bessel function with identical parameters for all three. The central portions of the beams on the experimental data are artificially limited because they exceed the limits of the 8 bit CMOS camera used to image the Bessel beam structure. The dimension of the central spot is constant and the concentric rings

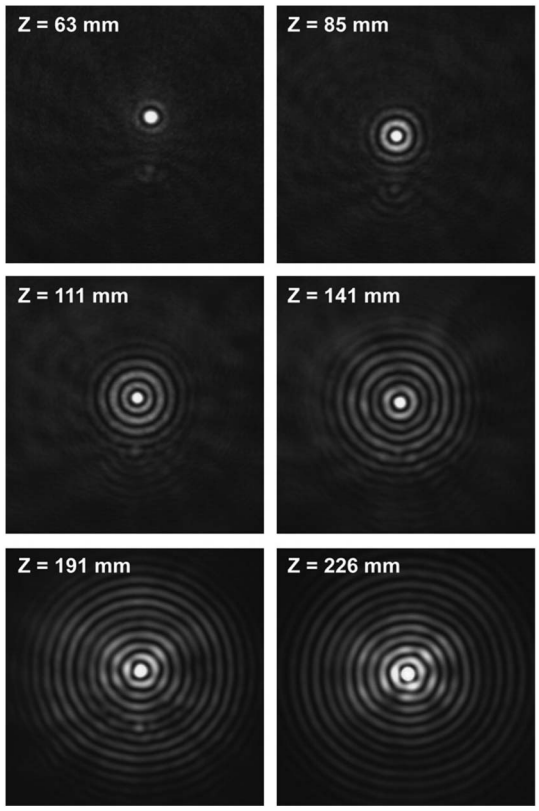

Fig. 2. Evolution of the spatial profile of the Bessel beam produced by a 0.50 mrad MLDM axicon along the propagation axis and recorded with the CMOS camera. Each image has a size of 1.56 mm × 1.56 mm.

remain at fixed positions. The first zero appears at 9.5 pixels, corresponding to a Bessel beam having an angle of

$$\beta = \frac{2.4048\lambda}{2\pi r_0} = 5\,\text{mrad}, \tag{3}$$

considering that r_0 is 9.5 pixels × 5.2 μm/pixel. Taking into account the telescope demagnification and that $\beta = 2\alpha$, this value is consistent with the cone angle of 0.5 mrad that was targeted for the reflecting surface of the MLDM. The central spot would correspond to a Gaussian beam with a beam size of ~85 μm and the collimation length extends over 350 mm, meaning that it is approximately 10 times longer than the Rayleigh range associated with the equivalent Gaussian spot size. Figure 4(a) shows a three-dimensional surface rendering of the mirror that was set to emulate an axicon with a cone angle of ~0.5 mrad. A plane cut of the associated axicon profile is shown in Fig. 4(b). Clearly, the surface profile represents a conical surface with a distortion well in the subwavelength range; the measured rms error of the surface profile, relative to a perfect conical shape, is 0.16 μm, i.e., it represents an accuracy of $\lambda/4$. Part of the rms error from the best cone fit was found to be attributable to a small tilt of the conical shape about its axis. The largest displacement

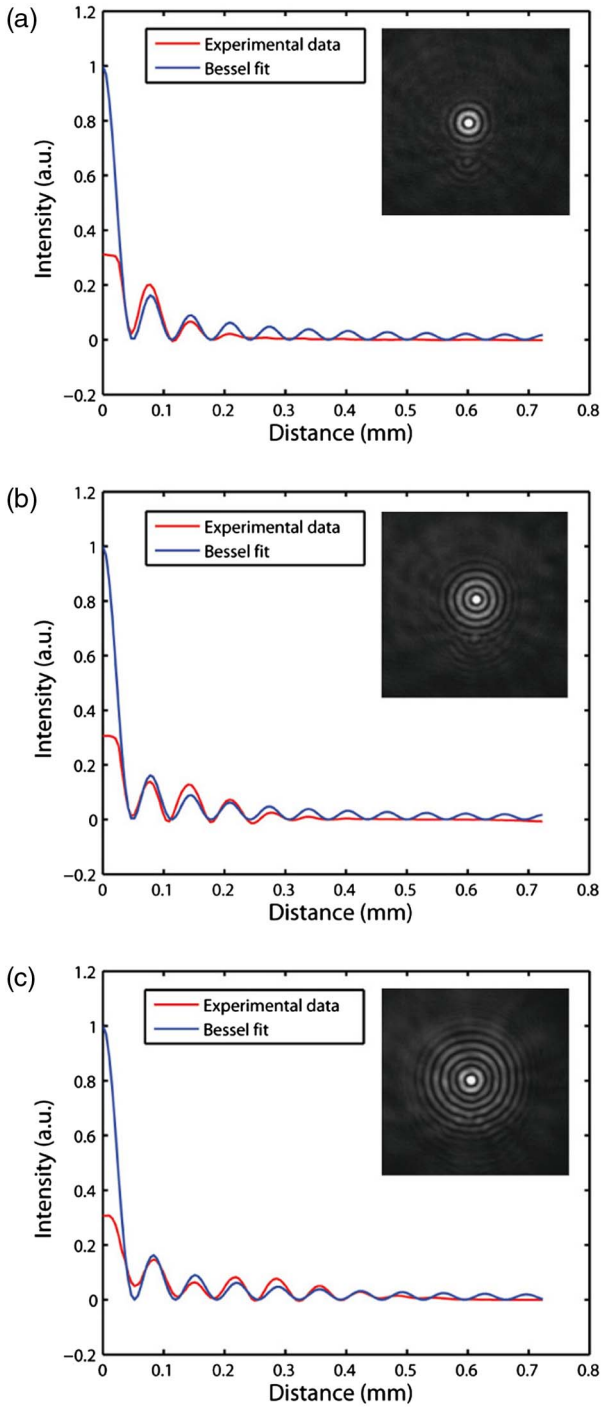

Fig. 3. (Color online) Mean radial intensity of the measured beam profile at three positions along the propagation axis ($z = 85$, 111, and 151 mm) and fitted using the same Bessel beam profile.

(sag) of a conical surface that we have produced is 15 μm, corresponding to a cone angle of 1.5 mrad; this value could be increased if we were not limited by the WFS dynamic range and the demagnifying telescope that reduces the maximum measurable slope, and also by increasing the Maxwell bobbin current. It should also be noted that the surface so produced is essentially of conical shape over almost its entirety. In particular, the central portion is still conical

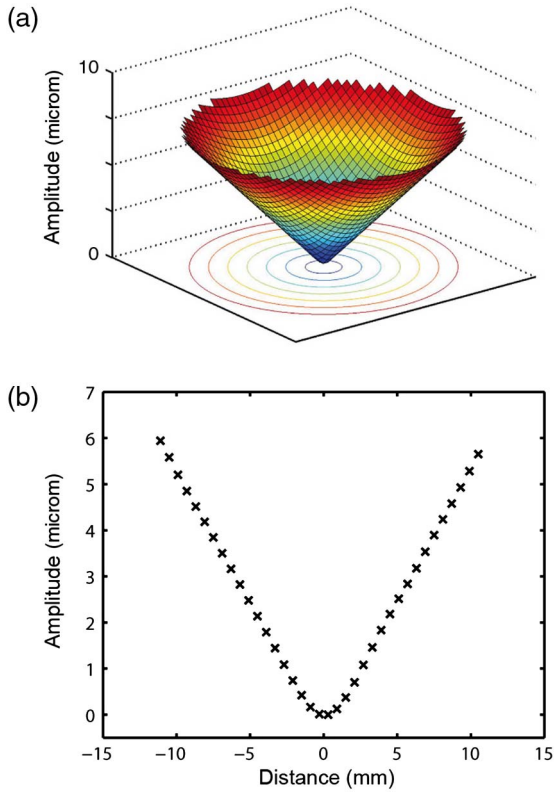

Fig. 4. (Color online) (a) Surface of a 0.5 mrad axicon produced by the MLDM and recorded by the WFS. (b) Plane cut of (a) showing the cone tip.

except near the immediate vicinity of the tip of the cone. This residual distortion takes place over an area covering less than 1% of the mirror surface.

In the far field, Bessel beams evolve into a thin annulus whose radius scales with the axicon angle. A typical far-field beam image and its intensity profile are shown in Fig. 5(a); the observed profile is consistent with the fact that a Bessel beam is the Fourier transform of a thin annular beam. Figure 5(b) shows the far-field beam image and intensity profile computed using the Fourier transform of the axicon surface that was recorded using the WFS. The computed profile shape is consistent with the profile of Fig. 5(a), but the annular ring is thinner. This is due to the fact that the axicon surface is optimized from the WFS data and that the light follows a different path in the optical setup. A possible improvement would be to find a proper metric that relates the quality of the far-field beam pattern to the currents sent to the coils. This way, the quality of the Bessel beams could be improved directly from the images recorded by the CMOS camera. Figure 6 shows that the radius of the far-field annulus (measured with a 300 mm focal length lens) agrees with the expected behavior to an excellent accuracy when the coils' currents are scaled (cone angle is linearly changed). It is important to appreciate the fact that in order to produce a Bessel beam with different central spot size and collimation length, it suffices to change the currents driving the 91 actuators by

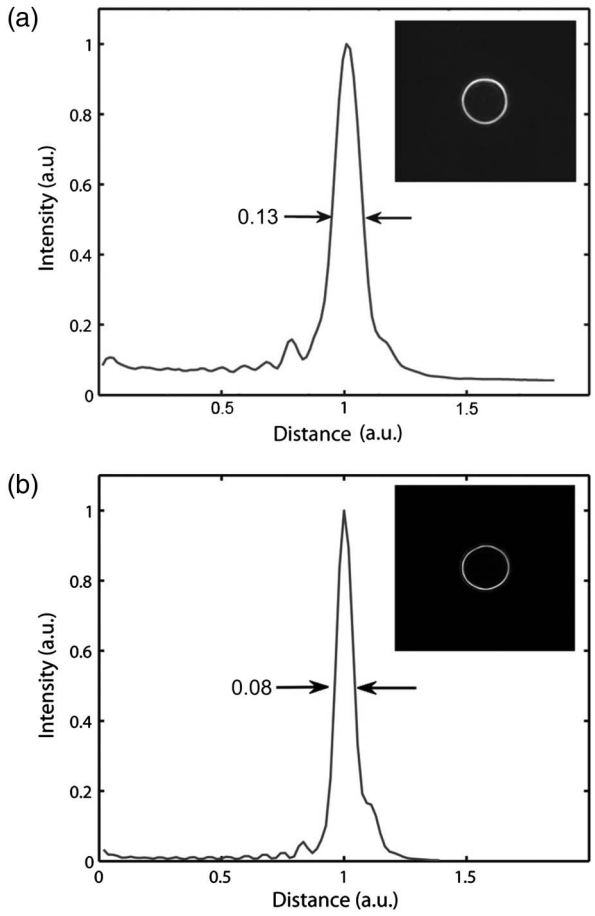

Fig. 5. (a) Observed far field produced by a 0.50 mrad MLDM axicon and imaged on the CMOS camera by a 300 mm focal length lens (insert). (b) Computed far-field distribution and simulated image (insert) using the Fourier transform of the conical surface recorded by the WFS. Both plots show a radial mean of the intensity distribution. The FWHM of the rings is given in relative units of the ring radius.

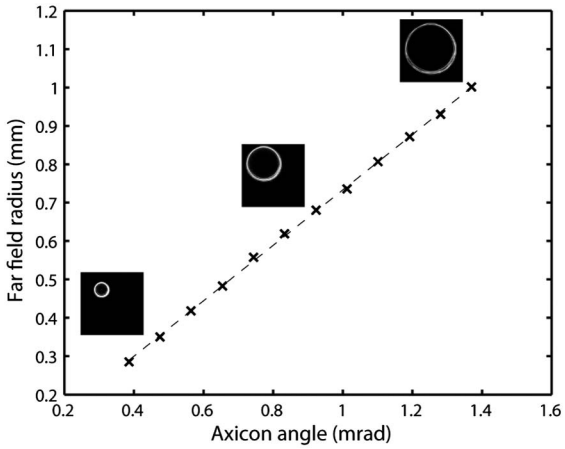

Fig. 6. Measured radius of the annular far-field beam as a function of the different axicon cone angles produced by the MLDM through a linear scaling of the currents that were used to produce a 0.5 mrad axicon cone angle. The values of the angles are computed from the surface maps recorded by the WFS.

a constant factor. The liquid mirror can be reconfigured in real time and convergence to a fully stable profile is achieved in about a tenth of a second.

4. Conclusion

In summary, we have shown that the magnetically controlled surface of a ferrofluid can be shaped in such a way as to behave as an effective axicon with an adjustable cone angle. Bessel beams produced by such an axicon have been characterized and the measured profiles are consistent with theory. In the experiments reported herein, we have demonstrated that the MLDM technology can produce conical surfaces with angles exceeding 1 mrad. In principle, the cone angle could be pushed to much higher values since displacements in the millimeter range can be achieved by ferrofluids. In this paper, we have used an MLDM to produce converging axicons, but diverging axicons could also be generated. Furthermore, other types of axicons with surface profiles that depart from ideal cones can be synthesized. Such profiles could be used to produce laser beams with a long and curved focal line, or to adjust the profile of the on-axis beam intensity distribution. MLDMs could also be used for the spatiotemporal reshaping of ultrashort pulses where they could adjust the phase of spatially dispersed spectral components [12,13].

Experiments on the reproducibility of the conical surfaces on an MLDM over time have not been done with conical surfaces. However, previous experiments done on the reproducibility of surfaces consisting of Zernike polynomials have been performed using a ZYGO interferometer. These experiments have shown that the same set of currents injected to the coils produces the same surface on the mirror to better than a tenth of a wavelength over a week. We expect the reproducibility of the MLDM to be this good over a few months unless the magnetic liquid is replaced. Vibrations did not raise any issue except when deliberately inducing them by touching the MLDM or the optical table. This lack of sensitivity to vibrations is due to the fact that the layer of magnetic liquid is thin (1 mm) and that the magnetic field of the coils, when the mirror is in function, stabilizes the surface of the liquid. Also, using a more viscous magnetic fluid would further improve the vibration sensitivity of the device.

Contrary to refractive axicons, spatial light modulators, or acousto-optic elements, our method does not depend upon the incident beam travelling through any material except the BK7 window, which could be removed; hence, in principle, the use of an MLDM does not raise issues about material damage and dispersion. Covering the mirror surface with a high reflectivity layer could pave the way to the potential use of the method with high peak power laser beams since the fraction of the incident beam that penetrates the material would be vanishingly small.

This work has been supported by grants from the Natural Sciences and Engineering Research Council of Canada (NSERC), the Canadian Institute for

Photonic Innovations (CIPI), and the Fonds québécois de la recherche sur la nature et les technologies (FQRNT).

References

1. A. Boivin, *Théorie et Calcul des Figures de Diffraction de Révolution* (Presses de l'Université Laval, 1964).
2. J. Durnin, J. J. Miceli, Jr., and J. H. Eberly, "Diffraction-free beams," Phys. Rev. Lett. **58**, 1499–1501 (1987).
3. V. Garcés-Chavez, D. McGloin, H. Melville, W. Sibbett, and K. Dholakia, "Simultaneous micromanipulation in multiple planes using a self-reconstructing light beam," Nature **419**, 145–147 (2002).
4. F. O. Fahrbach, P. Simon, and A. Rohrbach, "Microscopy with self-reconstructing beams," Nat. Photonics **4**, 780–785 (2010).
5. J. A. Kim, K. I. Lee, H. R. Noh, W. Jhe, and M. Ohtsu, "Atom trap in an axicon mirror," Opt. Lett. **22**, 117–119 (1997).
6. V. Garcés-Chavez, K. Volke-Sepulveda, S. Chavez-Cerda, W. Sibbett, and K. Dholakia, "Transfer of orbital angular momentum to an optically trapped low-index particle," Phys. Rev. A **66**, 063402 (2002).
7. M. Fortin, M. Piché, and E. F. Borra, "Optical tests with Bessel beam interferometry," Opt. Express **12**, 5887–5895 (2004).
8. B. Vohnsen, S. Castillo, and D. Rativa, "Wavefront sensing with an axicon," Opt. Lett. **36**, 846–848 (2011).
9. P. Dufour, M. Piché, Y. De Koninck, and N. McCarthy, "Two-photon excitation fluorescence microscopy with high depth of field using an axicon," Appl. Opt. **45**, 9246–9252 (2006).
10. T. A. Planchon, L. Gao, D. E. Milkie, M. W. Davidson, J. A. Galbraith, C. G. Galbraith, and E. Betzig, "Rapid three-dimensional isotropic imaging of living cells using Bessel beam plane illumination," Nat. Methods **8**, 417–423 (2011).
11. V. Zambon, R. Forest, N. McCarthy, and M. Piché, "Inscription of optical waveguides with ultrafast Bessel beams," in *Conference on Lasers and Electro-Optics/Quantum Electronics and Laser Science Conference and Photonic Applications Systems Technologies*, OSA Technical Digest (CD) (Optical Society of America, 2007), paper JTuA66.
12. M. A. Porras and P. Di Trapani, "Localized and stationary light wave modes in dispersive media," Phys. Rev. E **69**, 066606 (2004).
13. M. Dallaire, N. McCarthy, and M. Piché, "Spatiotemporal Bessel beams: theory and experiments," Opt. Express **17**, 18148–18164 (2009).
14. P. Polynkin, M. Kolesik, J. Moloney, G. Siviloglou, and D. Christodoulides, "Extreme nonlinear optics with ultra-intense self-bending Airy beams," Opt. Photon. News **21**(9), 38–43 (2010).
15. J. H. McLeod, "The axicon: a new type of optical element," J. Opt. Soc. Am. **44**, 592–597 (1954).
16. D. McGloin, G. C. Spalding, H. Melville, W. Sibbett, and K. Dholakia, "Three-dimensional arrays of optical bottle beams," Opt. Commun. **225**, 215–222 (2003).
17. I. Golub, "Fresnel axicon," Opt. Lett. **31**, 1890–1892 (2006).
18. V. Vaicaitis and S. Paulikas, "Formation of Bessel beams with continuously variable cone angle," Opt. Quantum Electron. **35**, 1065–1071 (2003).
19. G. Milne, G. D. M. Jeffries, and D. T. Chiu, "Tunable generation of Bessel beams with a fluidic axicon," Appl. Phys. Lett. **92**, 261101–261103 (2008).
20. E. McLeod, A. B. Hopkins, and C. B. Arnold, "Multiscale Bessel beams generated by a tunable acoustic gradient index of refraction lens," Opt. Lett. **31**, 3155–3157 (2006).
21. X. Wang, H.-T. Dai, and K.-S. Xu, "High efficient tunable fractal axicon based on LCoS," Chin. Phys. Lett. **25**, 985–988 (2008).
22. S. R. Mishra, S. K. Tiwari, S. P. Ram, and S. C. Mehendale, "Generation of hollow conic beams using a metal axicon mirror," Opt. Eng. **46**, 084002 (2007).
23. R. de Saint-Denis, E. Cagniot, P. Leprince, M. Fromager, and K. Ait-Ameur, "Low cost adjustable axicon," Optoelectron. Adv. Mater. **2**, 693–696 (2008).
24. P. Laird, E. F. Borra, R. Bergamesco, J. Gingras, L. Truong, and A. Ritcey, "Deformable mirrors based on magnetic liquids," Proc. SPIE **5490**, 1493–1501 (2004).
25. D. Brousseau, E. F. Borra, M. Rochette, and D. Bouffard-Landry, "Linearization of the response of a 91-actuator magnetic liquid deformable mirror," Opt. Express **18**, 8239–8250 (2010).
26. A. Iqbal and F. B. Amara, "Modeling of a magnetic-fluid deformable mirror for retinal imaging adaptive optics systems," Int. J. Optomechatron. **1**, 180–208 (2007).
27. J. C. Maxwell, *Treatise on Electricity and Magnetism* (Clarendon, 1873).